The Hydrated Electron

John M. Herbert and Marc P. Coons

Department of Chemistry and Biochemistry, The Ohio State University, Columbus,
Ohio 43210; email: herbert@chemistry.ohio-state.edu

Keywords

aqueous electron, water cluster anions, radiation chemistry, DNA damage

Abstract

Existence of a hydrated electron as a byproduct of water radiolysis was estab-
lished more than 50 years ago, yet this species continues to attract significant
attention due to its role in radiation chemistry, including DNA damage, and
because questions persist regarding its detailed structure. This work provides
an overview of what is known in regards to the structure and spectroscopy of
the hydrated electron, both in liquid water and in clusters $(H_2O)_N^-$, the latter
of which provide model systems for how water networks accommodate an ex-
cess electron. In clusters, the existence of both surface-bound and internally
bound states of the excess electron has elicited much debate, whereas in bulk
water there are questions regarding how best to understand the structure of
the excess electron's spin density. The energetics of the equilibrium species
$e^-(aq)$ and its excited states, in bulk water and at the air/water interface, are
also addressed.

1. INTRODUCTION

1.1. History

The nature of the solvated electron is an old question. The first observation of what would eventually be understood, more than a century later, as a solvated electron dates to Humphry Davy, in whose laboratory notebooks from 1808 can be found a description of the "beautiful metallic appearance" and "fine blue colour" observed when potassium crystals are heated in the presence of ammonia vapor (1). Following the liquefaction of ammonia, the blue color of sodium/ammonia mixtures was noted by Weyl in 1864 (2), who attributed the blue color to formation of a chemical compound, $NaNH_3$. This idea held sway for some time until convincing evidence against it was finally presented by Kraus in 1908 (3), in experiments originally intended to test the idea that electrons are the charge carriers in metallic conduction (4). The existence of dissolved ions as the charge carriers in electrolyte solutions had been established much earlier by Kohlrausch (5), but in Kraus's view, "knowledge of the solid state of matter . . . is far too limited to enable us to determine the nature of the processes which are specifically involved when electricity passes through a metal" (4, p. 1558), and he supposed that solutions of metals in nonconducting solvents might provide simpler systems on which to test theories of electrical conduction in metals.

To this end, Kraus measured the electrical conductivity of solutions of alkali metals dissolved in liquid ammonia, and already in the first of these papers (in 1908), he proposed that the charge carriers were "electrons surrounded by an envelope of ammonia" (6, p. 1332), i.e., solvated electrons, formed via the dissociation equilibrium $Na \rightleftharpoons Na^+ + e^-$. This inference seems all the more profound when one considers that the nature of the electron as the charge carrier in cathode ray tubes had been established only about ten years earlier (7), and Kraus's 1908 paper predates the publication of Millikan's oil drop experiment (8).

A few years after Kraus's proposal, Gibson & Argo (9, 10) measured optical absorption spectra of solutions of alkali and alkaline earth metals dissolved in liquid ammonia and in organic amines. These solutions each exhibit a strong blue color, and the wavelength of maximum absorption in a given solvent is independent of the identity of the metal (10). Based on the classical theory of dispersion in metals, Gibson & Argo showed that the absorption cross sections could not be reconciled with the conductivity data under the assumption that only the undissociated metal was present in solution (9). With this, the notion of a solvated electron as a distinct chemical species was established. These experiments predate the development of the "new" quantum theory, but by 1946 the idea had been put forward that the optical spectra of alkali metal solutions in ammonia arises from $s \rightarrow p$ excitation of a particle in a quasi-spherical solvent void (11). This notion was later elaborated (12) and adapted for the aqueous electron (13) by Jortner and co-workers.

This review focuses on the specific case of the solvated electron in water, $e^-(aq)$, for which detailed historical accounts of early experiments can be found elsewhere (14–16). Briefly, as early as 1952 it was suggested that such a species might be a byproduct of the radiolysis of aqueous solutions (17), but reaction of alkali metals with water does not produce any visible coloration, which is ultimately a consequence of the fact that the lifetime of $e^-(aq)$ in neutral water is ∼300 μs when generated in low concentrations and can be significantly shorter under other conditions (18). Aqueous electrons can be generated by pulsed radiolysis of aqueous solutions (18), as in the original 1962 measurement of the optical spectrum (19); by sonolysis of aqueous solutions (20); by two-photon laser excitation of liquid water; or else by photodetachment of a suitable electron donor, e.g., by accessing charge-transfer-to-solvent excited states of $I^-(aq)$ or $CN^-(aq)$ (21–23). In the 50+ years since it was first detected experimentally, $e^-(aq)$ has come to be recognized as one of the primary radicals formed upon radiolysis of water (14, 24, 25).

Theoretical attempts to understand the detailed structure of $e^-(aq)$ are nearly as old as the first measurement of the optical spectrum. Early models were continuum or semicontinuum in nature (13, 26–29) and assumed that the electron inhabits an excluded volume in the structure of liquid water, consistent with experimental measurements of the partial molar volume of $e^-(aq)$ (30, 31). In the 1970s, analysis of electron spin resonance (ESR) spectra of electrons trapped in glassy alkaline water seemed to confirm this picture (32). The same picture would later emerge from atomistic simulations using one-electron (pseudopotential) models (33, 34), and finally from first-principles calculations based on density functional theory (DFT) (35–37). As such, this cavity model of $e^-(aq)$ has become the conventional paradigm, although not without occasional (and ongoing) controversy (38–42), as discussed in Section 4.

In the 1980s, finite cluster analogues of the hydrated electron, $(H_2O)_N^-$, were created in a molecular beam (43), and the possibility of mass-selecting these clusters and interrogating them spectroscopically provides another avenue to understanding how water accommodates an extra electron. Interpretation of the cluster spectroscopy has proven controversial (44–46) and is discussed in Section 2. Spectroscopic studies of $e^-(aq)$ in liquid water are discussed in Section 3.

Cavity model:
a model in which the aqueous electron creates and occupies a quasi-spherical region of excluded volume within the solvent

Vacuum level:
reference energy of a noninteracting electron removed from the solvent

1.2. Chemical Significance

Although this review focuses mainly on structural, spectroscopic, and energetic considerations, the importance of $e^-(aq)$ as a potent reducing agent in aqueous chemistry cannot be overstated. **Figure 1** illustrates some of the early-time events in water radiolysis (47), whereupon ionizing radiation generates three primary radicals: $H^\bullet$, $HO^\bullet$, and $e^-(aq)$. The latter thermalizes on a picosecond timescale, $\sim$3.5 eV below vacuum level, and its formation and depletion are readily monitored via an intense absorption at 720 nm that is ascribed to $s \rightarrow p$ excitation within the excluded volume of the cavity occupied by $e^-(aq)$.

Although some reactions involving $e^-(aq)$ are diffusion-limited, many exhibit activation energies of 1–8 kcal/mol (24), suggesting that the kinetics is controlled by the availability of a vacant orbital on the reacting partner species. However, even for the simplest reaction,

$$H^+(aq) + e^-(aq) \rightarrow H^\bullet(aq), \qquad 1.$$

the molecular-level mechanism is not always clear. Whereas a long-held view is that $e^-(aq)$ always reacts via an electron-transfer mechanism (14), recent DFT simulations of reaction (1) in small water clusters suggest that it may occur via proton transfer into the $e^-(aq)$ cavity (48, 49). This requires significant (and simultaneous) rearrangement of both the proton and the electron hydration shells, including considerable distortion of the unpaired electron that facilitates reaction but comes with an energetic penalty for desolvation of the two hydrophilic reactants. Perhaps surprisingly, Reaction 1 proceeds more slowly than $H^+(aq) + HO^-(aq) \rightarrow H_2O$, where one might anticipate similar disruption of the solvation shells around the two ions, and also more slowly than $e^-(aq) + HO^\bullet(aq) \rightarrow HO^-(aq)$. These examples suggest that not all $e^-(aq)$ chemistry should be conceptualized in electron-transfer terms.

Direct absorption of ionizing radiation can induce mutagenic lesions in DNA; however, it is actually secondary species such as $e^-(aq)$ generated in water that cause the most damage (50–52). Electrons with kinetic energies in the range 3–20 eV can induce single and double strand breaks in vacuum (53), with a damage profile peaking around 10 eV that suggests core-excited resonances of a nucleobase may be involved (52, 53). In addition, electrons with energies as low as 0.1–2.0 eV, well below the estimated 7.0–10.5 eV ionization threshold of DNA (53), can induce covalent bond cleavage in DNA. In the proposed mechanism (54), an electron is captured by a π^* orbital of a DNA base forming an anion shape resonance, with excess kinetic
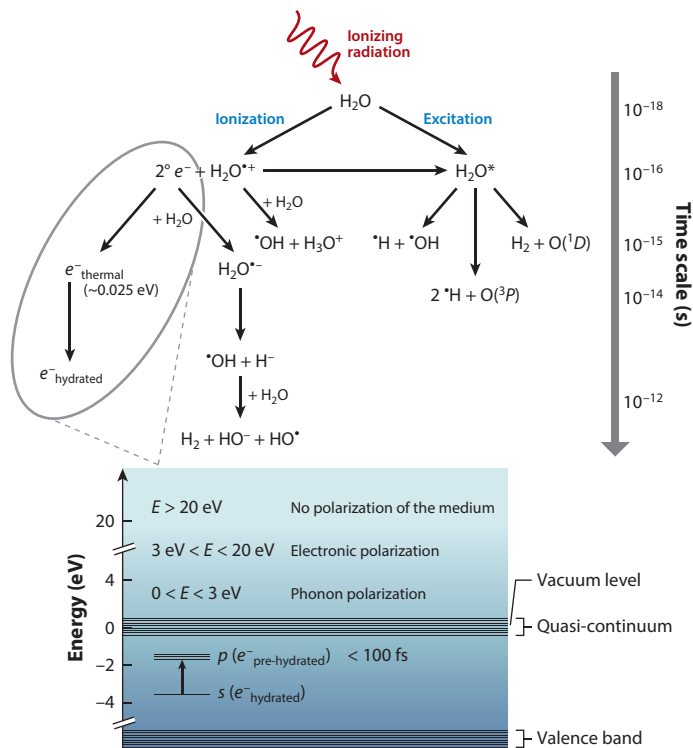
Figure 1

Schematic overview of water radiolysis, wherein ionizing radiation generates radical intermediates $e^-(aq)$, $H^\bullet$, and $HO^\bullet$. An energy-level diagram of $e^-(aq)$ in bulk water is depicted in the lower part of the figure. Figure adapted from Reference 47 with permission. Copyright 2012 American Chemical Society.

energy of the incident electron inducing an additional $\pi \to \pi^*$ excitation: $e^- + (\pi)^2 \to (\pi)^1(\pi^*)^2$. The resulting $(\pi)^1(\pi^*)^2$ state is dissociative along the sugar–phosphate $\sigma(CO)$ bond coordinate. Electrons in aqueous solution have been observed to form anion resonances in DNA on an ultrafast timescale (55), with subsequent DNA degradation within a few picoseconds. Whereas electron attachment to nucleobases in the gas phase is energetically unfavorable, addition of just a few solvating water molecules results in a dramatic ($\gtrsim 1$ eV) increase in the adiabatic electron affinities of both nucleobases and nucleotides (56, 57). As such, one may expect electron attachment to DNA to be enhanced in aqueous environments.

2. WATER CLUSTER ANIONS, $(H_2O)_N^-$

Finite-size $(H_2O)_N^-$ clusters were first produced in a molecular beam in 1981 (43), and since that time clusters up to $N = 200$ have been interrogated by photoelectron spectroscopy (58–60) and those up to $N = 50$ by vibrational spectroscopy (61, 62). Clusters, especially small ones, are amenable to accurate electronic structure calculations that can elucidate electron binding motifs, by locating those isomers that reproduce experimental spectra. A major goal in cluster studies is therefore to understand, in molecular-level detail, how the water network accommodates the extra electron and how this accommodation changes as the cluster evolves from a few molecules into something that might be analogous to $e^-(aq)$. Even for clusters as small as $(H_2O)_6^-$, however,

theoretical assignment of the experimental spectra has proven challenging and remains an open question for larger clusters. As described below, the number of isomers that are potentially in play is such that one may reasonably question whether computational studies that simply catalog isomers are genuinely useful. Studies of larger clusters may yield insight about the condensed phase, but this probably requires abandoning the notion of assigning distinct structural isomers to observed spectral features. We illustrate the complexity of this problem with a case study of $(H_2O)_6^-$, then address a long-standing controversy regarding the interpretation of photoelectron spectra in larger isomers and, in particular, the existence of surface-bound versus internally bound cluster isomers.

2.1. Small Clusters: Direct Comparison to Ab Initio Calculations

The evolving interpretation of the structure of $(H_2O)_6^-$ provides a good example of the difficulty in assigning cluster isomers based on vertical electron binding energies (VEBEs), which for $(H_2O)_6^-$ were first measured in 1996 (63). The measured VEBE spectrum (**Figure 2**) consists of two main peaks that isotopic substitution reveals to be the band origins of two distinct isomers. On the basis of ab initio VEBE calculations for various $(H_2O)_6^-$ isomers, this spectrum was immediately assigned by Kim et al. (64) to the two isomers depicted in **Figure 2a**. The computed VEBEs differ by <0.1 eV from the experimental values, and this assignment was consistent with early
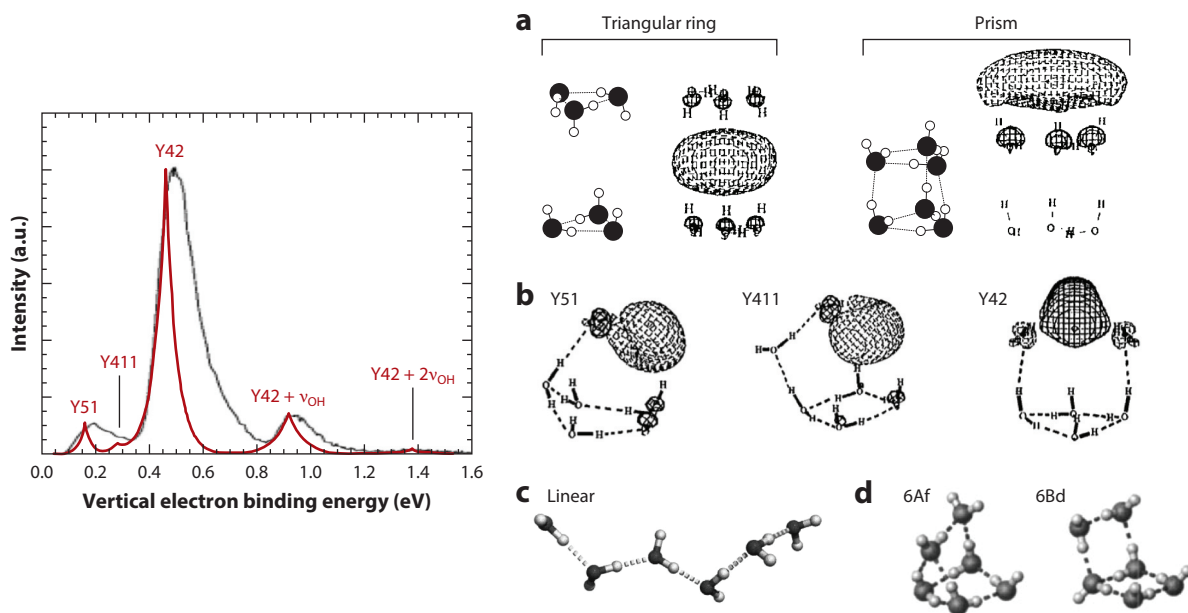

Figure 2

(*Left*) Experimental VEBE spectrum of $(H_2O)_6^-$ (*black*) overlaid with a computed spectrum based on ab initio calculations (*red*). Putative assignments for the peaks are labeled according to the cluster isomers depicted on the right. Experimental spectrum adapted from Reference 63 with permission; copyright 1996 American Chemical Society. Simulated spectrum adapted from Reference 65 with permission; copyright 1997 American Institute of Physics. (*Right*) Cluster isomers that have been implicated in these spectra, from 1996 to 2003 (64–69). Panel *a* adapted from Reference 68 with permission from Elsevier. Panel *b* adapted from Reference 65 with permission; copyright 1997 American Institute of Physics. Panel *c* adapted from Reference 66 with permission; copyright 1999 American Institute of Physics. Panel *d* adapted from Reference 67 with permission; copyright 2003 American Institute of Physics. Abbreviation: VEBE, vertical electron binding energy.

speculation (58) regarding the existence of both surface-bound and internally bound cluster isomers. Nevertheless, this assignment was quickly revised by the same authors (65), based on a more exhaustive search, to consist of three different isomers that are depicted in **Figure 2b**. For this new assignment, a simulated distribution of VEBEs that includes the effects of vibrational broadening is in semiquantitative agreement with experiment, as shown in **Figure 2**. However, Jordan and co-workers (66) later revisited the calculations using a higher-quality basis set that modifies the VEBEs by ≈0.15 eV, and ultimately concluded that the spectrum likely originates from the linear isomer shown in **Figure 2c**. A few years later, Kim and co-workers (67) recomputed VEBEs using higher levels of theory and reassigned the spectrum to the two isomers depicted in **Figure 2d**.

This example highlights the pitfalls inherent to assigning structural isomers based on VEBEs alone, but vibrational spectroscopy can provide additional information. Vibrational predissociation spectra for $Ar_n(H_2O)_6^-$ clusters (66, 70, 71) reveal an intense O–H stretch doublet that is redshifted up to ~400 cm^{-1} relative to gas-phase H_2O; see **Figure 3a**. This feature was used, in part, to assign the linear isomer to the VEBE spectrum in **Figure 2**, because linear isomers reproduce the intense, strongly redshifted doublet in the O–H stretching region (66).

As is often the case, however, the $(H_2O)_6^-$ vibrational spectrum arises from multiple isomers with strongly overlapping vibrational signatures; these can be deconvoluted from one another by exploiting the fact that the population ratio changes as a function of the number of attached Ar atoms (70, 71). Deconvoluted spectra for two distinct isomers of $(D_2O)_6^-$ are shown in **Figure 3b,c**, where they have been assigned to isomers based on scaled harmonic frequencies computed using DFT. The ab initio vibrational spectra are in excellent agreement with experiment, even though the VEBEs computed at the same level of theory are far too large, for reasons that are understood (72). Unfortunately, this means that it is difficult to use a consistent yet computationally tractable theoretical approach for both vibrational and photoelectron spectra, especially as the cluster size grows much beyond $N = 6$. Ultimately, the 6Af/6Bd assignment of the photoelectron spectrum (**Figure 2d**), originally proposed by Lee et al. (67) in 2003 and reaffirmed in later assignments of vibrational predissociation spectra (70, 71), has emerged as the consensus view, even upon more exhaustive searching of the potential energy surface (73, 74). This consensus, however, was 10 years in the making and came more than 15 years after the first photoelectron spectrum of $(H_2O)_6^-$ was reported.

For the incrementally larger $(H_2O)_7^-$ cluster, scaled harmonic frequencies fit just as well to several structures having comparable relative energies but that differ in some of the details of the hydrogen-bond arrangement (75). As cluster size grows beyond this, attempts to make definitive isomer assignments quickly become a losing proposition, and perhaps the best that one can do is to assign the local geometry associated with a particular vibrational signature (75, 76). The strongly redshifted O–H stretching feature in $(H_2O)_6^-$ is a good example and has been assigned to a water molecule in a double hydrogen-bond acceptor (AA) configuration (see **Figure 3b**). In the AA water molecule, neither O–H moiety participates in hydrogen bonding to other water molecules, and both are free to form hydrogen bonds to the unpaired electron instead. The large redshift in the O–H stretching modes on this AA water molecule arises from penetration of the unpaired electron into $\sigma^*(OH)$ orbitals (77). The vibrational signature of the AA water molecule persists in $(H_2O)_N^-$ vibrational spectra up to at least $N = 21$ (61), with some evidence of it up to $N = 35$ (62).

The difficulty in assigning spectra to individual isomers arises in no small part due to the fact that the relevant experiments generally probe nonequilibrium ensembles. There is no guarantee that the isomers observed are in fact the lowest-energy ones, even in cold molecular beams, due to significant energy deposition upon electron attachment as well as the existence of autodetachment channels that may preclude experimental observation of certain isomers found in a
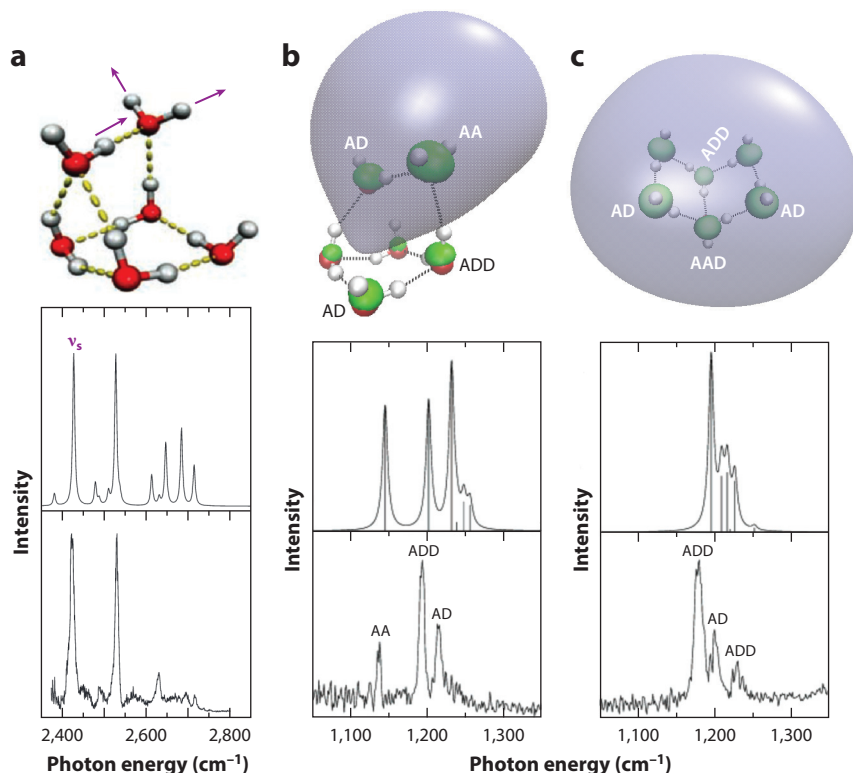
Figure 3

Vibrational spectra of $(D_2O)_6^-$ from experiment (*bottom*) and from scaled DFT harmonic frequencies (*middle*). (*a*) Spectra in the O–D stretching region, with an illustration of the very intense symmetric AA stretching mode, ν_s. (*b*) Deconvoluted spectra of the AA isomer in the O–D bending region. (*c*) Deconvoluted spectra of the "book" isomer in the O–D bending region. In panels *b* and *c*, the singly occupied molecular orbital is shown as well, in blue and green at a 50% isoprobability contour. Water molecules are labeled as AA, AAD, etc., based on their hydrogen-bonding environment (acceptor or donor) within the water network. Spectra in the bending region adapted from Reference 70 with permission; copyright 2005 American Chemical Society. Spectra in the stretching region adapted from Reference 71 with permission from AAAS. Abbreviation: DFT, density functional theory.

computational search. The complexity of the situation is again illustrated by $(H_2O)_6^-$, for which Jordan and co-workers (73, 74) have performed exhaustive sampling using a one-electron model. A disconnectivity graph, representing various local minimum and the transition structures that connect them, is shown in **Figure 4** and reveals 41 local minima within 10 kJ/mol of the global minimum! Vibrational predissociation experiments exploiting isotopic substitution reveal that it is the book isomer of $(H_2O)_6^-$ that is formed initially upon electron attachment in the molecular beam, whereas the AA isomer is formed subsequently (78). A pathway that connects these isomers while avoiding autodetachment can be located, but passes through no fewer than 13 intermediate local minima (74).

The important lesson from this expansive view of the $(H_2O)_6^-$ potential energy surface is that most of the low-lying isomers are not observed in vibrational predissociation experiments, although theory suggests they may exist fleetingly as intermediates. This makes it exceedingly difficult to connect theory to experiment in order to elucidate individual structural isomers and implies that
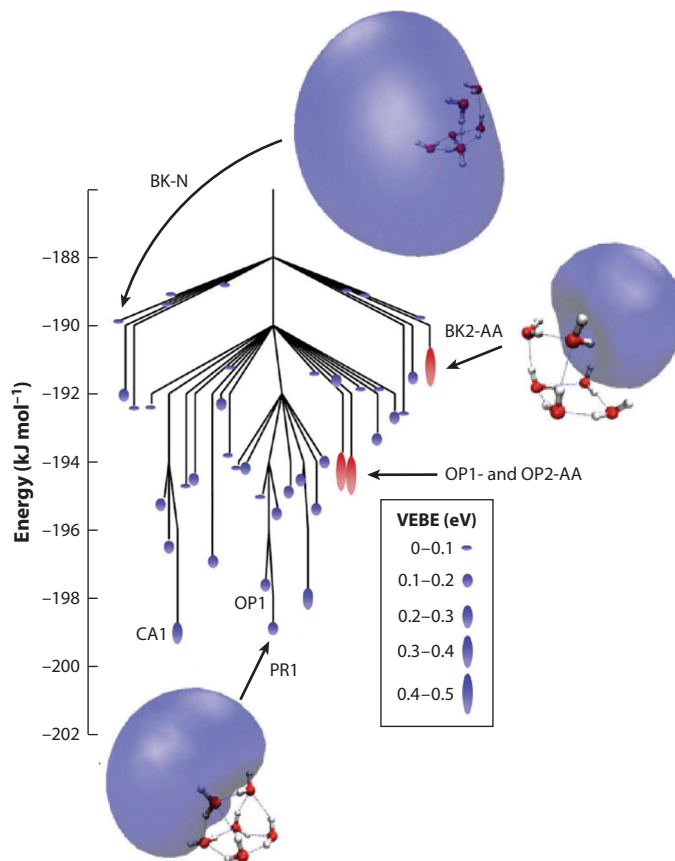
Figure 4

Low-energy portion of the disconnectivity graph for $(H_2O)_6^-$. Endpoints of the branches indicate local minima, and branching points represent the transition states that connect them. Some of the minima are labeled according to structural motif: book (BK), prism (PR), cage (CA), or open prism (OP), with AA-type isomers indicated explicitly. For each local minimum, the size of the colored ellipse indicates the magnitude of the VEBE, with AA-type structures labeled in red and non-AA isomers labeled in blue. Starting from the BK-N isomer initially formed in the molecular beam (78), an autodetachment-free pathway to the OP1-AA and OP2-AA isomers that are also observed experimentally can be found, but it passes through a total of 13 intermediate local minima including the CA1, OP1, and PR1 minima (74). Disconnectivity graph adapted from Reference 74 with permission from Elsevier. Abbreviation: VEBE, vertical electron binding energy.

in much larger clusters than $(H_2O)_6^-$, it is probably foolish to try to assign experimental spectra to individual cluster isomers.

2.2. Larger Clusters: Surface Versus Internal States

In larger $(H_2O)_N^-$ clusters there is an ongoing debate regarding the nature of the transition, as a function of cluster size, from an electron bound at the cluster surface into something that might reasonably be taken as a finite analogue of the aqueous electron in bulk water. Theoretical calculations by Barnett et al. (79, 80) that predate the first experimental photoelectron spectra predicted the existence of both surface-bound and internally (cavity-)bound cluster isomers in the
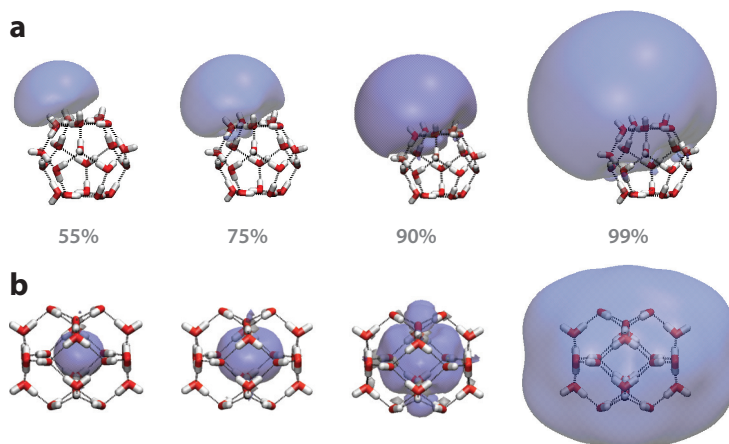
Figure 5

Isoprobability contours of the singly occupied molecular orbitals in (*a*) a surface-bound isomer of $(H_2O)_{20}^-$ and (*b*) a cavity-bound isomer of $(H_2O)_{24}^-$, each with similar VEBEs of ~ 1 eV. Each isosurface contains the indicated fraction of the probability density. Figure adapted from Reference 82 with permission. Copyright 2008 American Chemical Society. Abbreviation: VEBE, vertical electron binding energy.

size range of $N = 32$–64. Modern ab initio calculations demonstrate unambiguously that both types of isomers exist (81, 82); representative examples are depicted in **Figure 5**. Note that even in the internally bound case, visual inspection suggests that the tail of the cavity-centered wave function penetrates perhaps two solvation shells, and simulations of $e^-(aq)$ with cavity-forming pseudopotential models suggest that the hydrogen-bond network is indeed disrupted in the first two solvation shells but converges to that of bulk water in the third shell (83). Thus, even one-electron models exhibit much of the complex structure, such as significant electron density in the interstices between water molecules, that has been noted in ab initio calculations (37).

Experimental VEBEs from photoelectron spectra (58–60) of size-selected $(H_2O)_N^-$ clusters are plotted as a function of $N^{-1/3}$ in **Figure 6**. The choice of $N^{-1/3}$ is an attempt to connect the cluster data to $e^-(aq)$ in bulk water, as within a simple Born-type solvation model, wherein the electron inhabits a small spherical cavity of fixed size centered in a homogeneous dielectric sphere of radius R, the VEBE varies as R^{-1}, and $R \propto N^{1/3}$ for large, spherical clusters. Later analysis revealed, however, that continuum electrostatics also predicts VEBEs that vary as R^{-1} for surface-bound electrons (86), hence the scaling behavior of the VEBEs is inconclusive as to binding motif.

Photoelectron spectra measured in these experiments exhibit multiple peaks that are presumed to arise from different isomers, with relative populations that are sensitive to the source conditions of the molecular beam (59). Data series labeled I, II, and III in **Figure 6a** were obtained using conditions that should correspond to beam temperatures $T_I > T_{II} > T_{III}$ (59). All three data series vary roughly as $N^{-1/3}$, although the isomer II data change slope in the $N = 30$–50 range. One source of controversy has been that the isomer I data, presumed to represent the internally solvated electron because no clusters with larger VEBEs are observed experimentally (87), are in excellent agreement with theoretical calculations for surface-bound cluster isomers (44, 59), whereas the calculations place the internally solvated $(H_2O)_N^-$ clusters at higher VEBEs (59). However, none of the early one-electron models is quantitative for prediction of VEBEs (83, 88), and ad hoc scaling of the VEBEs computed by Barnett et al. affords good agreement between isomer I and
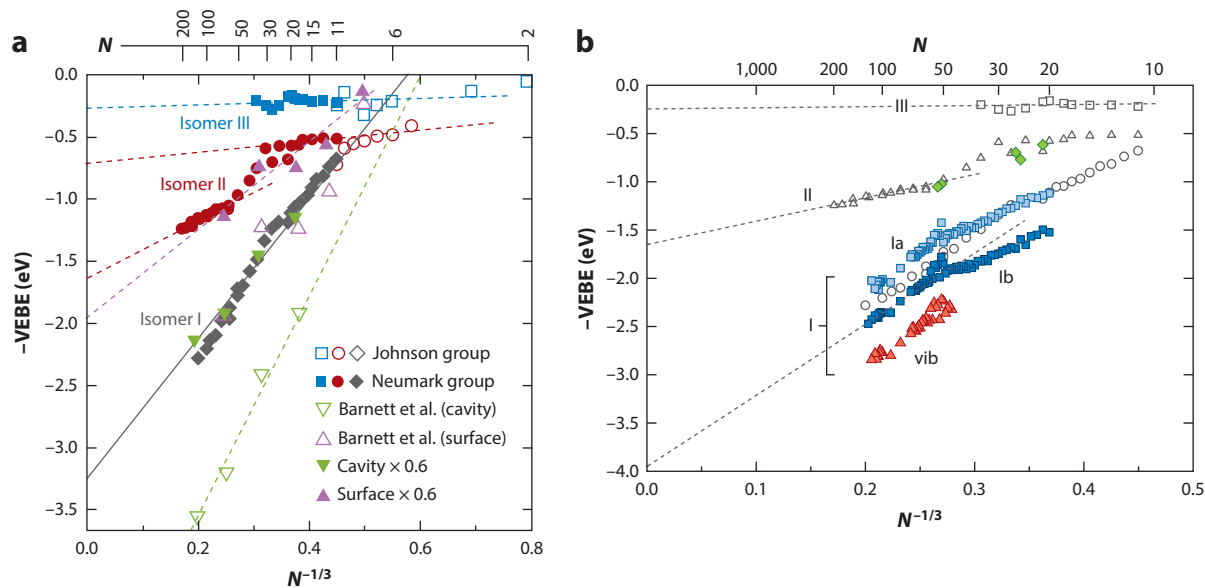
Figure 6

VEBEs for size-selected $(H_2O)_N^-$ clusters. (*a*) Experimental values from the Neumark group (59), measured via photoelectron spectroscopy, and from the Johnson group (70, 84, 85), measured mostly using infrared predissociation spectroscopy. The Neumark data for isomer I are essentially the same as those measured earlier by the Bowen group (58). Theoretical values calculated by Barnett et al. (79) are also shown as originally reported, and as scaled by an ad hoc factor of 0.6 as suggested in Reference 59. Panel *a* adapted from Reference 59 with permission from AAAS. (*b*) Data from the Neumark group (59) (*open symbols*) plotted against more recent measurements in cold clusters from the von Issendorff group (60), who labeled two of their data series as Ia and Ib and assigned the third series (labeled vib) to vibrational excitation of an O–H stretch upon photodetachment of the electron. Panel *b* adapted from Reference 60 with permission. Copyright 2009 American Institute of Physics. Abbreviation: VEBE, vertical electron binding energy.

the predicted cavity-bound isomers, whereas VEBEs for surface-bound electrons are in good agreement with isomer II (59) (see **Figure 6a**).

More recent experiments, in which the $(H_2O)_N^-$ clusters are cooled in an ion trap following electron attachment, reveal new data series "Ia" and "Ib" that appear to bracket the original isomer I data (see **Figure 6b**). These newer data suggest that earlier experiments, in which the temperature is not well characterized, may have observed a transition between isomers Ia and Ib. In light of these new data, the cluster problem was revisited using a pseudopotential model that is quantitative for prediction of VEBEs as compared with high-level ab initio calculations (83). Several classes of isomers were located in simulations of cluster anions in the range of $N = 20–200$ (89). These are illustrated for the case $N = 40$ in **Figure 7** and include dipole-bound isomers (whose VEBEs are very small and can be assigned as isomer III without controversy); surface-bound isomers with larger VEBEs; and also cavity-type isomers. New in these simulations is a distinction between the surface-bound species, in which the electron is bound by dangling O–H moieties rather than simply by the overall cluster dipole moment (as in the dipole-bound case), and a partially embedded isomer, in which H_2O molecules at the cluster surface have reoriented themselves to form a partial solvation shell around the unpaired electron.

Much like the experiments, the simulated cluster ensembles are highly sensitive to initial conditions, but are nevertheless in semiquantitative agreement with the cold cluster ion data in **Figure 6b** (89). Juxtaposition of the simulated and measured VEBE versus $N^{-1/3}$ plots suggests that isomer II is the canonical surface-bound species, whereas the strongest-binding isomer, Ib, agrees well with
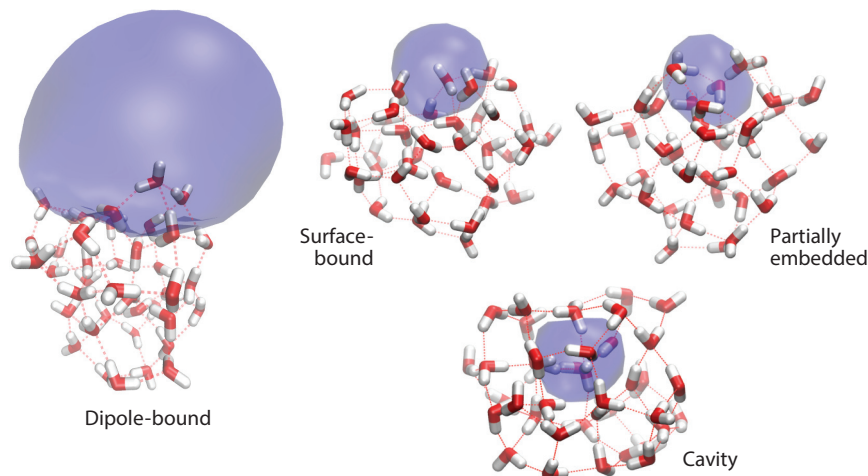
Figure 7

Illustration of four classes of $(H_2O)_{40}^-$ cluster isomers. In each case, the indicated isocontour encapsulates 70% of $|\psi|^2$ for the unpaired electron. In the dipole-bound isomer, at most one O–H group is hydrogen-bonded to the electron, and binding arises mainly from the overall cluster dipole moment, resulting in a relatively diffuse electron. Surface-bound isomers are characterized by several O–H moieties that form hydrogen bonds to the electron. In the partially embedded case, additional reorientation forms a partial solvation shell, so that the electron remains localized at the cluster surface but is similar in its compactness to the internalized, cavity-bound species. Figure adapted from Reference 89 with permission. Copyright 2011 American Chemical Society.

theoretical results for the cavity-bound isomers, with agreement that improves as the simulated clusters are warmed up and allowed to anneal (89), as in the ion-trap experiments that afford the data in **Figure 6b**. In between isomers II and Ib lies isomer Ia, which the simulations suggest could be the partially embedded species (89).

3. AQUEOUS ELECTRON, $e^-(aq)$

The structure of the hydrated electron in liquid water has been a topic of ongoing debate for decades. Early theoretical models posited a particle in a spherical cavity (13, 26–29), a model that, in its modern ab initio version, is remarkably successful in describing both the spectroscopy and the thermodynamics of $e^-(aq)$ (90–92). Various experiments (32, 93) support a model in which one O–H moiety from each of several H_2O molecules is directly hydrogen-bonded to the $e^-(aq)$ charge distribution (spin density), and this picture has been repeatedly confirmed by atomistic simulations (33, 35–37, 83, 94). An early six-coordinate model (**Figure 8a**) put forward by Kevan on the basis of ESR measurements in low-temperature alkaline glasses (32) has more recently yielded to a four-coordinate picture (**Figure 8b**) (83, 92, 94). Here, we summarize efforts to understand the structure and dynamics of $e^-(aq)$, both in bulk liquid water and also at the air/water interface. This discussion is organized along the lines of the spectroscopic techniques that have been used to investigate this species.

3.1. Photoelectron Spectroscopy

For water cluster anions, photoelectron spectroscopy is arguably the least incisive technique for elucidating binding motifs, as evidenced by the examples in Section 2. Nevertheless, the ability to
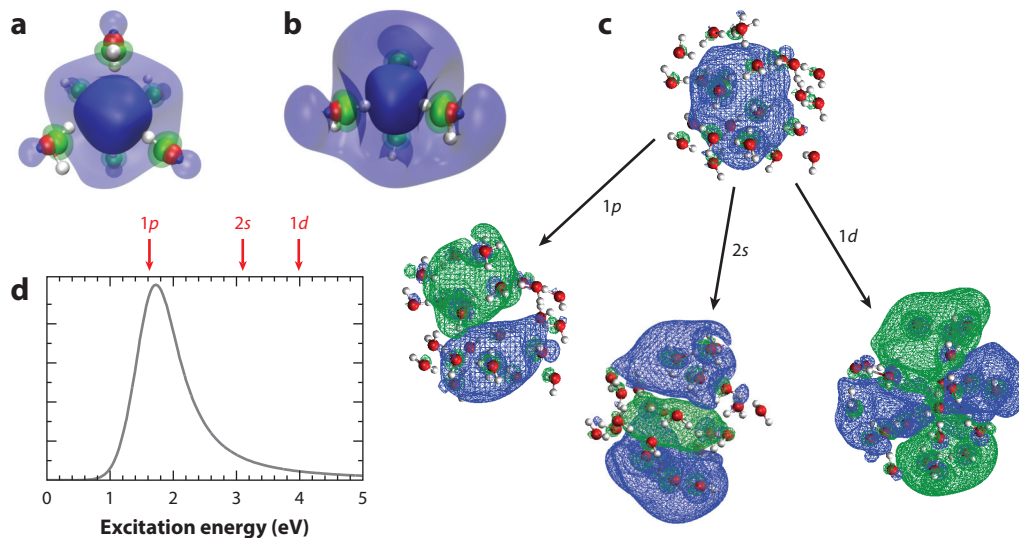
Figure 8

(*a*) Kevan's (32) six-coordinate model for $e^-(aq)$ and (*b*) the four-coordinate model of Kumar et al. (92), both depicted here as the singly occupied molecular orbital computed at the Hartree–Fock/6-31++G* level with dielectric continuum boundary conditions. Translucent and opaque isosurfaces encapsulate 40% and 80% of the probability density, respectively, with the green color (opposite in sign to the blue color) indicating where the tail of the electron's wave function penetrates into the frontier orbitals of the water molecules. (*c*) Natural transition orbitals describing excitations of $e^-(aq)$. The depicted isocontours encapsulate 90% of the probability density in each case. (*d*) The experimental absorption spectrum, indicating the energy levels for excitations of the particular snapshot that is shown in panel *c*. Panel *c* adapted from Reference 95 with permission. Copyright 2010 American Chemical Society.

measure the VEBE of $e^-(aq)$ in bulk water using liquid microjet photoelectron spectroscopy (96–101) serves as an important check on extrapolations of cluster photoelectron spectra. The consensus from these experiments is that the VEBE lies in the range of 3.3–3.7 eV, with most values in the range of 3.3–3.4 eV (101), which is entirely consistent with cluster extrapolations (102) and with simulations using a pseudopotential model that includes self-consistent electron–water and water–water polarization (83).

In one particular microjet experiment, however, a feature at 1.6 eV is observed with a lifetime $\gtrsim$100 ps and is attributed to $e^-(aq)$ bound at the water/vacuum interface (99). Although this value is similar to both the 1.4-eV VEBE that is measured at the surface of amorphous solid water (103) and also the extrapolation of the cluster photoelectron data for isomer II (**Figure 6a**), attempts by others to duplicate this result at the liquid/vapor interface have found only a transient feature with a lifetime of ~100 fs (98, 100). This includes experiments performed at low electron kinetic energies, for which the electron attenuation length is relatively short (104) and thus the spectrum should be dominated by the signal from species bound at the interface (100). Given an $s \rightarrow p$ excitation energy of 1.7 eV and a bulk VEBE of 3.3–3.4 eV, a short-lived feature having a VEBE of 1.6 eV is consistent with a transient excited state of $e^-(aq)$ or possibly a hot precursor sometimes called the presolvated electron (47, 55). This does not, however, explain the longer-lived signal observed in Reference 99 with a ~100-ps lifetime. This is inconsistent with the measured internal conversion lifetime of 60–75 fs (105, 106). Nevertheless, speculation has arisen that a putative interfacial electron at 1.6 eV below vacuum level might play a role in the radiation chemistry of DNA, and specifically, that the much lower VEBE at the interface might provide the proper energetics for dissociative electron attachment to DNA, resulting in single strand breaks (99,

107–110). This hypothesis requires that the interfacial species possess an energy ≤ 2.5 eV below vacuum level (107, 108), which is inconsistent with simulation data, suggesting that the VEBE at the interface is quite similar to the bulk value (111). Moreover, simulations in which an electron is introduced at an equilibrated air/water interface suggest that the electron dissolves into bulk solution within ∼30 ps (111), as depicted in **Figure 9**, with no more than a shallow free-energy minimum at the interface (112).

Simulations also suggest that within ∼10 ps of its introduction at the interface, the electron is sufficiently solvated so that its VEBE is very similar to that predicted for $e^-(aq)$ in bulk water. Ab initio calculations including more than 80 quantum-mechanical water molecules predict an interfacial VEBE of 3.1–3.2 eV, versus 3.4–3.5 eV for the bulk species (111). This suggests not only that liquid microjet photoelectron spectroscopy is likely incapable of distinguishing the bulk versus interfacial signal, but also, more importantly, that neither species appears to have the proper energetics to induce dissociative electron attachment to DNA (111).

The situation is very different on ice surfaces. Experiments by Wolf and co-workers (103, 113, 114) on amorphous solid water support a picture that is not entirely dissimilar from the $t = 0$ snapshot in **Figure 9**, in which a "balloon" of probability density is weakly tethered to the surface, possibly occupying a Bjerrum defect (113). The signal from this putative interfacial electron is quenched when a layer of Xe atoms is deposited on the ice surface (103, 113, 114), supporting the notion of a binding motif wherein the electron extends significantly beyond the interface. On the surface of amorphous solid water, the signal for $e^-(aq)$ persists on a timescale of minutes (113) and can induce dissociative electron attachment in chlorofluorocarbons (114). This may suggest a role for hydrated electrons in atmospheric chemistry occurring on ice particles (115–117), in which the electrons are generated by cosmic rays, although this claim remains controversial (118, 119).

3.2. Vibrational Spectroscopy

As with clusters, vibrational spectroscopy often proves to be a more incisive probe of structure than does photoelectron spectroscopy, and resonance Raman spectroscopy of $e^-(aq)$ in isotopically substituted water provides important structural information. For $e^-(aq)$ dissolved in H_2O or D_2O, the water bending region consists of a single peak, but in mixtures of H_2O and D_2O this peak is split in a manner suggesting that only a single O–H moiety per H_2O molecule coordinates to the electron (93). This is consistent with the structural models obtained from most atomistic simulations of $e^-(aq)$, e.g., those in **Figure 8**, but is inconsistent with models in which the H_2O dipole vector is oriented toward the electron. It would also seem to be inconsistent with models in which the electron is delocalized across one or more water molecules (38, 120, 121).

The hydrated electron at the air/water interface has been examined using surface-sensitive vibrational spectroscopy (122, 123). One set of experiments was performed both with and without a layer of surfactant molecules, with the idea that their presence should disrupt the structure of any surface-bound electron that extends significantly beyond the interface, such as the one in the $t = 0$ snapshot of **Figure 9**. However, when the polar part of the surfactant is small (the hydroxyl moiety of decanol), no change in the spectroscopy is observed relative to that of a surfactant-free interface, but the signal changes significantly when the polar group is large (122). The authors conclude that the putative interfacial hydrated electron might reside 1–2 nm into solvent (122), near enough to the interface to lift inversion symmetry and thus afford a signal, yet far enough away (according to simulations such as those shown in **Figure 9**) that its structure is very much like that of $e^-(aq)$ in bulk water. Unlike ice, where the signal attributed to the interfacial electron persists on a timescale of minutes, these experiments suggest that the interfacial signal survives for ≈750 ps (122) or perhaps ≲100 ps (123).
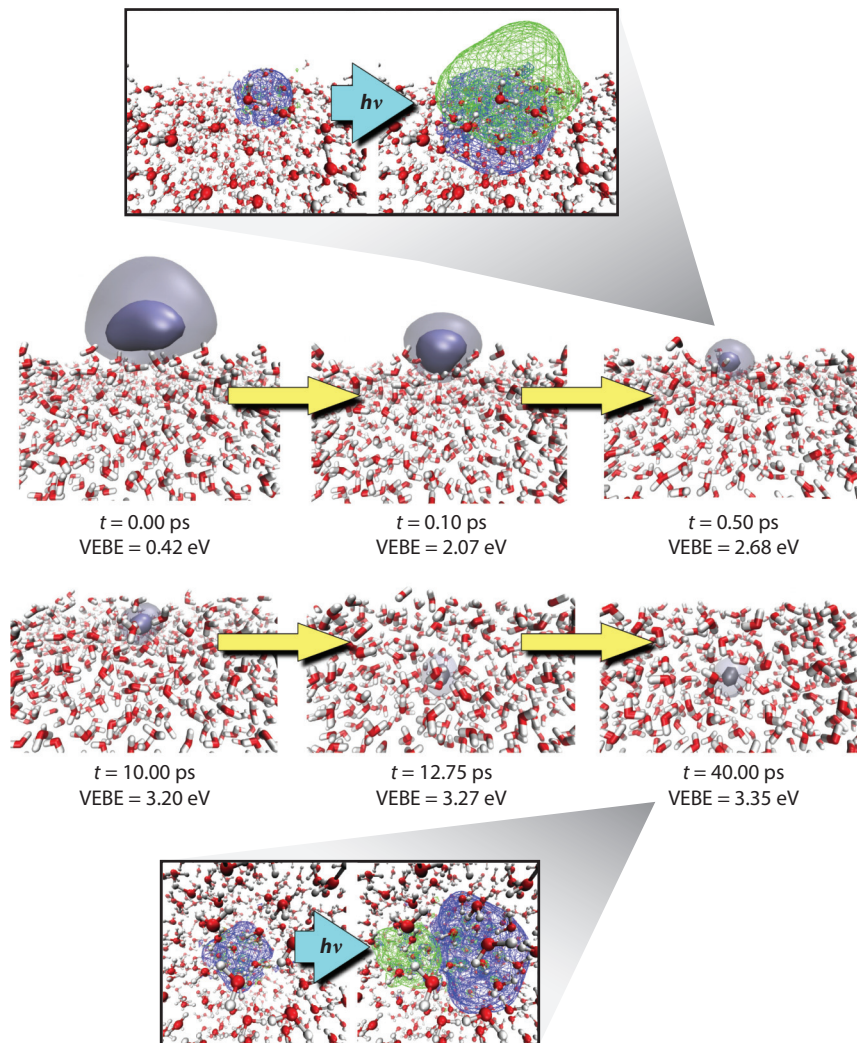
Figure 9

Evolution of the hydrated electron from the air/water interface into bulk solution. At $t = 0$ the electron localizes in a surface trap arising from dangling O–H moieties at the interface, but within $\sim$10 ps it forms a species that is essentially indistinguishable, spectroscopically speaking, from $e^-(aq)$ in bulk water and dissolves into bulk solution within $\sim$30 ps. Opaque and translucent isosurfaces encapsulate 50% and 95% of the probability density, respectively. Callouts depict DFT natural transition orbitals associated with the lowest $s \rightarrow p$ excitation, based on calculations reported in Reference 91. Figure adapted from Reference 111 with permission. Copyright 2016 American Chemical Society. Abbreviations: DFT, density functional theory; VEBE, vertical electron binding energy.

3.3. Optical Spectroscopy

Perhaps the most salient feature of $e^-(aq)$ is its electronic absorption spectrum, which is a primary means by which this species is monitored. The spectrum is plotted in **Figure 8d** and has been experimentally characterized under a variety of thermodynamic conditions (124). It exhibits a Gaussian line shape on the red edge and a Lorentzian line shape on the blue edge (102), features

that are also apparent in electronic spectra of $(H_2O)_N^-$ clusters (125). Much has been made of the "blue tail" in this spectrum, as this feature is not reproduced in most theoretical calculations (126). Given the Lorentzian line shape (suggestive of lifetime broadening), along with the fact that the blue edge of the absorption spectrum overlaps the red edge of the photoelectron spectrum (127, 128), this tail has long been attributed to bound → continuum transitions (27, 127, 129). This, however, does not fully explain the absence of a tail in theoretical calculations, many of which use real-space grids and are capable of describing continuum states, in principle. In contrast, calculations using a one-electron model that includes self-consistent electron–water polarization do reproduce the blue tail (83, 95), and these calculations suggest that at least some of the states in the tail are highly delocalized, quasi-continuum wave functions that are nevertheless bound states, in the sense that the excited-state energy lies below vacuum level (95, 130). In these calculations, the polarization response of the water molecules plays a crucial role in amplifying the oscillator strengths of the states in question. This is interesting in view of a measured value of 1.14 for the integrated oscillator strength of the $e^-(aq)$ absorption spectrum (131). A value >1 implies that excitation of $e^-(aq)$ is not strictly a one-electron transition but rather some intensity is borrowed from electrons on water molecules.

Despite this (quantitatively minor) complexity, the main part of the optical spectrum can be understood in terms of a particle-in-a-box model. This is evident from the time-dependent DFT (TDDFT) natural transition orbitals depicted in **Figure 8c**, which were computed from atomistic, all-electron simulations yet can easily be assigned particle-in-a-cavity quantum numbers. The lowest three excitations resemble dipole-allowed $1s \rightarrow 1p$ transitions, and these three transitions account—essentially quantitatively—for the main, Gaussian part of the optical spectrum, as shown in **Figure 10a**. (Unlike the case of a one-electron atom, within the spherical cavity model the principle quantum number places no restriction on angular momentum, hence $1p$ states do exist.) Because the cavity in the atomistic simulations is ellipsoidal and fluxional, the $1s \rightarrow 1p$ transitions are heterogeneously broadened, accounting for the width of the spectrum. The $1s \rightarrow 2s$ excitations
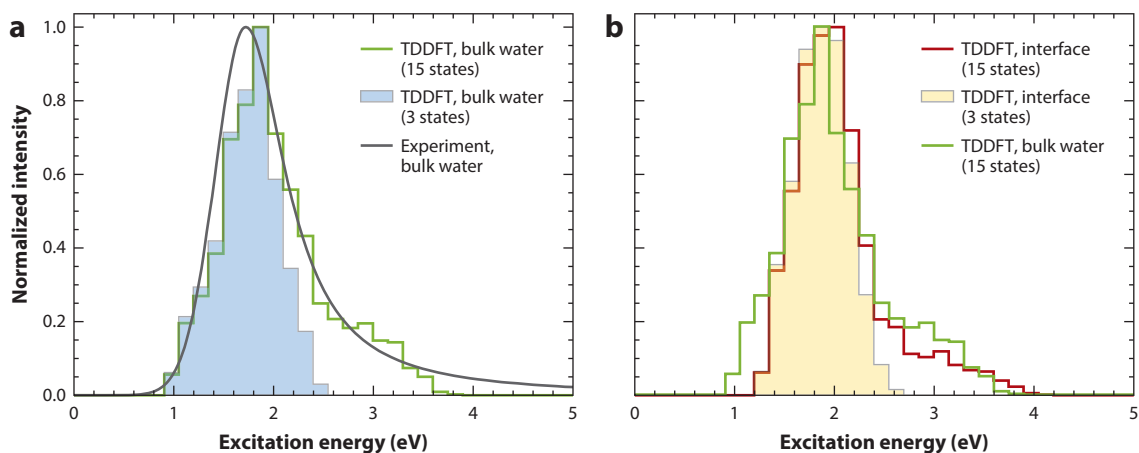
Figure 10

Optical absorption spectrum of the hydrated electron (*a*) in bulk water, where the experimental spectrum is overlaid with results of TDDFT calculations, and (*b*) at the water/vacuum interface, where only the TDDFT results are available. In panel *b* the computed interfacial spectrum is overlaid with the bulk spectrum computed at the same level of theory, for comparison. Two different theoretical calculations are shown: one using the lowest 3 excited states and the other using 15 excited states, in each case weighted by oscillator strength and using data from Reference 91. All spectra are normalized to unit intensity at their respective absorption maxima, but no fitting is employed in the calculations. Abbreviation: TDDFT, time-dependent density functional theory.
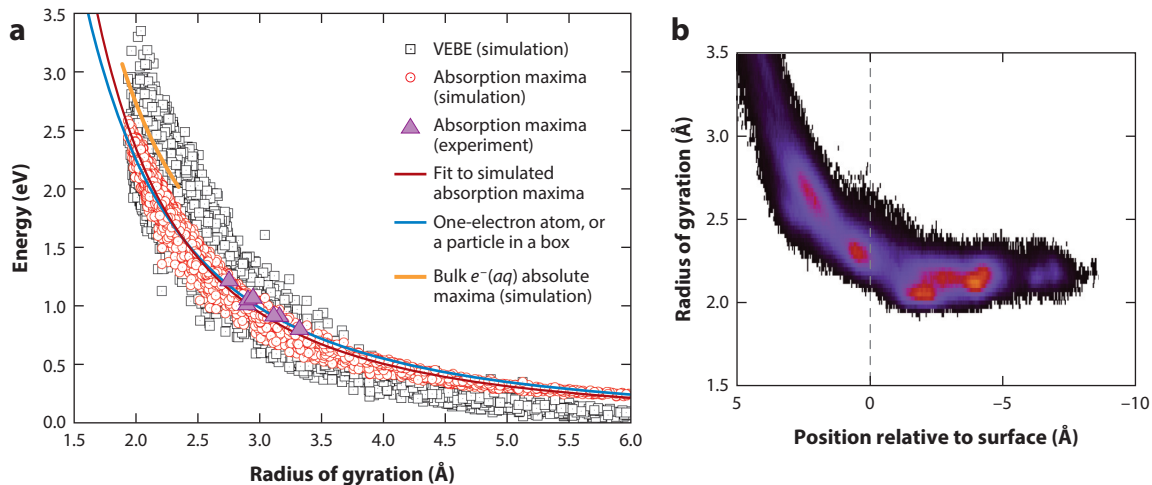
Figure 11

(*a*) Correlation between the electron's radius of gyration, r_g, and its VEBE (*gray squares*) and electronic absorption maximum, E_{max} (*red circles*), as obtained from $(H_2O)_N^-$ simulation data for $N = 20–200$ under a variety of conditions. Experimental results for E_{max} in clusters are also shown (*purple triangles*) along with simulation results for E_{max} of $e^-(aq)$ in bulk water (*orange curve*). The blue curve represents the lowest excitation energy for a one-electron atom as a function of r_g, and has nearly the same form as the analogous result for a particle in a spherical cavity (89). (*b*) Histogram showing how r_g converges as a function of the distance between the electron's centroid and the surface of the cluster, with negative values indicating an internalized electron. Figure adapted from Reference 89 with permission. Copyright 2011 American Chemical Society. Abbreviation: VEBE, vertical electron binding energy.

are dipole-forbidden for a rigorously spherical cavity, which explains the sharp falloff in intensity beyond the main $1s \rightarrow 1p$ band. Nevertheless, higher-lying transitions into $2s$, $1d$, and quasi-continuum orbitals borrow intensity from the $1s \rightarrow 1p$ excitations, so agreement with experiment across the whole spectral range requires the calculation of more than just the lowest three states (42, 83, 91, 95). As is evident from **Figure 10*a***, the lowest 15 TDDFT excited states will suffice.

Analytically solvable models predict that both the VEBE and the $1s \rightarrow 1p$ excitation energy are fully determined by the electron's radius of gyration,

$$r_g = \langle (\mathbf{r} - \langle \mathbf{r} \rangle) \cdot (\mathbf{r} - \langle \mathbf{r} \rangle) \rangle^{1/2}, \qquad 2.$$

and in particular vary as r_g^{-2}. This r_g^{-2} dependence emerges naturally in condensed-phase simulations of $e^-(aq)$ in bulk water (33, 37) but is even more evident in cluster data; see **Figure 11*a***. Both VEBEs and electronic absorption maxima for $(H_2O)_N^-$ clusters closely follow the r_g^{-2} curve that is predicted both by a particle-in-a-cavity model, as appropriate for an internally solvated electron, and by a one-electron atomic model that is more sensible for a surface-bound electron (89). Importantly, clusters sample a much wider range of r_g values than do the bulk simulations, so the robustness of these relationships across a wide array of $(H_2O)_N^-$ simulation data (89, 90) demonstrates that knowledge of r_g alone is sufficient to make a semiquantitative prediction of both the VEBE and the absorption maximum.

This relationship explains, for example, the rapid growth in the VEBE as the hydrated electron at the air/water interface becomes solvated (**Figure 9**), because formation of even a partial solvation shell at the interface localizes the electron to the point where its radius of gyration is not much different from that of the bulk species (111). This, too, is readily seen from cluster data, particularly in the plot in **Figure 11*b*** showing how r_g converges from values >3.5 Å, when the electron's

centroid is >5 Å from the cluster surface, to a value much closer to the bulk value ($r_g = 2.45$ Å) when the centroid of the electron reaches the interface.

Given this rapid convergence of r_g at the interface, and the fact that this property alone provides a good guess as to the optical absorption maximum, one might predict that the optical spectrum of $e^-(aq)$ at the air/water interface would not be dissimilar to that of $e^-(aq)$ in bulk water. The interfacial spectrum has not been measured, but it can be simulated and the result is shown in **Figure 10b**, superimposed upon the corresponding bulk-water calculation. The two spectra exhibit minor differences at most, and the absorption maxima are identical. Thus, there appears to be little difference between $e^-(aq)$ in bulk water versus the air/water interface, in terms of the photoelectron or the electronic absorption spectroscopy.

4. THEORETICAL MODELS

4.1. Canonical Cavity Model

Implicit in much of the discussion above is an assumption that the electron occupies an excluded volume in the structure of liquid water, in some version of a cavity model. Whereas Kevan (32), in 1981, proposed a six-coordinate model (**Figure 8a**) based on ESR experiments in alkaline, glassy water at $T = 77$ K, and furthermore noted that coordination numbers less than or equal to 4 were inconsistent with the ESR line shape (132), modern DFT (37) and pseudopotential simulations (83, 94) afford structures in neat water at $T = 300$ K that exhibit coordination numbers slightly greater than 4 (**Figure 8b**). These simulations (35, 36, 83, 133) are spontaneously cavity-forming within ~1 ps. It should be borne in mind that the cavity is highly fluxional at room temperature, collapsing and re-forming via librational motions of the water molecules (83, 134), consistent with the very fast diffusion of $e^-(aq)$. Amongst aqueous ions, diffusion of $e^-(aq)$ is somewhat slower than the Grotthuß-assisted diffusion of $H^+(aq)$ but comparable with that of $OH^-(aq)$, whose Grotthuß-type diffusion is also aided by librational motions (135). Diffusion of $e^-(aq)$ is three times faster than that of $K^+(aq)$, based on ion mobility measurements (136). Water's librational motion at the air/water interface is similar to that in bulk water (137), consistent with the short lifetime of $e^-(aq)$ at the interface.

The cavity model reproduces a wealth of experimental data quantitatively. These include the free energy of solvation (92), or in other words the adiabatic electron affinity of liquid water; the VEBE (83, 111); and the electronic absorption spectrum (83, 91, 95), including the blue tail and the line width, the latter of which can be converted into a radius of gyration ($r_g = 2.45$ Å) that is also consistent with both simulation data (83) and DFT calculations (92). Simulations also exhibit librational dynamics and hydrogen-bonding structure in the first solvation shell that are consistent with what is inferred from resonance Raman spectroscopy (83), namely, a single $O–H\cdots e^-$ hydrogen bond per water molecule, with a weakened restoring force for H_2O librations (93). DFT calculations reproduce the ~200 cm^{-1} redshift in the stretching frequency of the O–H bonds that are directly coordinated to the electron (92). Semiquantitative results are obtained for the diffusion coefficient (83, 134), including the temperature dependence thereof (134). Finally, DFT calculations on a four-coordinate cavity-type model structure afford semiquantitative values for the shift in the electron g-factor relative to its free-electron value (92) and for ESR hyperfine couplings (92, 138). Most of these features are reproduced by one-electron models (83), provided that the underlying water model is polarizable (130), although the vibrational frequency shifts, g-tensor shifts, and hyperfine coupling constants require orbitals on the water molecules, and thus a many-electron treatment is necessary to describe these properties.

Overwhelmingly, theoretical results and comparisons with experiment are consistent with a cavity-centered spin density, but one whose tail extends significantly into the solvent. This is evident already in $(H_2O)_N^-$ clusters (**Figure 5**), and calculations suggest that only 40–50% of the spin density is contained within the cavity itself (37, 82). Disruption of the hydrogen-bonding structure and dynamics extends into the second solvation shell but not into the third (83). Despite this favorable agreement, however, alternative structural models have been put forward over many years, as discussed below.

4.2. Solvent Anion Model

In 1991, Tuttle & Golden re-examined electronic spectra of both electrons and iodide anions in a variety of solvents (139), finding that the iodide spectra are largely insensitive to both temperature and solvent, whereas the electron's spectrum is sensitive to both. This observation served to revive previous proposals (120, 121) that the so-called solvated electron might be better conceptualized as a molecular anion.

Electron affinities of alkali metals, M, suggest that their anions M^- are stable in the gas phase (140), and polar solvents (S) should further stabilize these anions. The conjectured model (120) is composed of an equilibrium $M^+ + 2\ S^- \rightleftharpoons M^- + 2\ S$ between a metal and solvent anion as well as the ion-pairing processes $M^+ + M^- \rightleftharpoons M^+{\cdot}M^-$ and $M^+ + S^- \rightleftharpoons M^+{\cdot}S^-$. The solvent anion S^- is proposed to exist in place of a cavity-bound solvated electron. A continuum treatment of these equilibria affords qualitative agreement with experiment for the temperature dependence of the vapor pressure, conductivity, and NMR Knight shift (of ^{14}N) in metal–ammonia solutions (120), although it is not clear that a modern understanding of the cavity model is incompatible with Knight shifts of the solvent nuclei.

A major factor leading Tuttle & Golden to champion the model of a solvent-anion complex seems to have been the failure of 1980s-era electron–water pseudopotentials to correctly describe the position and shape of the $e^-(aq)$ absorption spectrum, although the peak position is now reproduced, without fitting, by newer models (83, 94). As further evidence, Tuttle & Golden (121, 139) cite the fact that the solvent-anion model explains the slight composition dependence of the solvated electron's optical spectrum in binary solvent mixtures, by means of a two-absorber model consisting of an equilibrium between a solvent anion in each of the two solvents: $S_1^- + S_2 \rightleftharpoons S_1 + S_2^-$. There has been no effort to simulate solvated electrons in mixed solvents and thus no reason to assume that a cavity-type model is necessarily restricted to a one-absorber model, as different local solvation environments might easily afford slightly different absorption spectra. Though it would be interesting to pursue this with the quantitative machinery of modern ab initio simulations, and though Tuttle & Golden saw "no compelling reason to afford solvated electrons a cavity-type . . . constitution" (139, p. 5735), in view of how successfully modern theory can explain the properties of $e^-(aq)$ based on a cavity model, we conclude there is no compelling reason, at present, to entertain the solvent-anion model.

4.3. Hydrated Hydronium Model

A somewhat different version of the solvent-anion model was advocated by Robinson and co-workers (136), in which the species responsible for the spectroscopic features ascribed to $e^-(aq)$ is actually a complex of H_3O and HO^-. This hypothesis has been revived more recently by Domcke & Sobolewski (108, 141), who propose a slightly different model in which $H_3O(aq)$ forms a zwitterionic complex $H_3O^+ \cdots e^-$ upon hydration, behavior that is evident in the singly
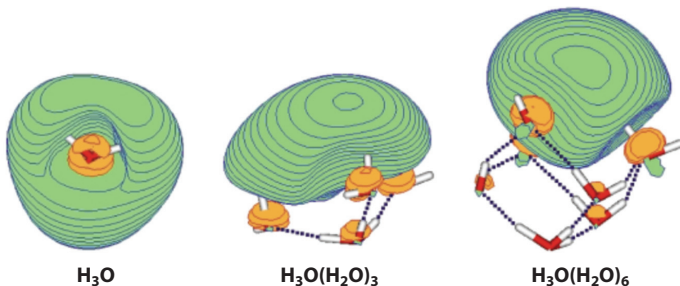
Figure 12

Singly occupied molecular orbitals for hydrated hydronium clusters. Figure adapted from Reference 141 with permission. Copyright 2002 PCCP Owner Societies.

occupied orbitals of $H_3O(H_2O)_N$ clusters (**Figure 12**). Upon addition of three water molecules, a $3s$ Rydberg-type orbital detaches from the H_3O core, leaving behind a hydronium ion as part of the hydrogen-bonding network. The lowest excitation energy (Rydberg $3s \to 3p$) shifts dramatically upon microhydration, from 2.2 eV to 1.5 eV, and the splitting of the degenerate $^2E(p_{xy})$ state of H_3O gives rise to $D_0 \to {^2}E(p_{xy})$ and $D_0 \to {^2}A(p_z)$ transitions that span the range 1.1–3.0 eV and have a combined oscillator strength of nearly unity (141), which is consistent with the optical spectrum attributed to $e^-(aq)$.

Vibrational frequencies (141) and resonance Raman intensities (142) have been computed for $H_3O(H_2O)_N$ clusters using DFT and exhibit particularly intense O–H stretching vibrations for the O–H moieties that coordinate directly to the singly occupied orbital. This is consistent with the charge-sloshing mechanism that explains the enhanced intensity of these vibrations in $(H_2O)_N^-$ clusters (77). Simulated resonance Raman spectra are in qualitative agreement with the measured resonance Raman spectrum of $e^-(aq)$ (93). Although these calculations have not been extended to clusters larger than $H_3O(H_2O)_9$, the fact that an electron charge-separates from the solvent molecules, and appears to hydrogen bond to one O–H moiety per water molecule, suggests that the hydrated hydronium model of $e^-(aq)$ may not be all that different from the cavity model.

4.4. Non-Cavity Model

In 2010, Larsen, Glover & Schwartz (LGS) reported an electron–water pseudopotential model that affords a qualitatively different balance between attractive and repulsive interactions and predicts a structure for $e^-(aq)$ that does not involve an excluded volume at all (38). Instead, water molecules permeate the unpaired electron's wave function such that the water density is greatest ($\rho = 1.23$ g/cm^3) near the electron's centroid. Nevertheless, the radius of gyration of this model's wave function ($r_g = 2.6$ Å) is close to the experimental value (2.45 Å), and because the size of the excess electron's wave function has been shown to be the key factor determining its excitation energy (89), it is not surprising that the LGS model reproduces the salient features of the absorption spectrum.

The non-cavity LGS model remains controversial (39–42). Enhanced water density in the region of the unpaired electron is difficult to reconcile with the fact that measurements of the partial molar volume of $e^-(aq)$ are positive when corrected for electrostriction effects (30, 143), a fact that has sometimes been misquoted in the literature as discussed in Reference 42. The most recent such measurement is consistent with a cavity radius of ≈ 2.2 Å (31). Furthermore, LGS

Non-cavity model: a model in which a solvated electron is delocalized over solvent molecules, without forming an excluded volume

wave functions for $(H_2O)_N^-$ clusters are qualitatively inconsistent with ab initio results (40). The LGS model is derived from exact pseudopotential theory applied to $(H_2O)^-$, as are two other cavity-forming models (83, 94), but after fitting the electron–water interaction potential to an analytic form, the LGS model affords a pseudo-orbital eigenvalue that is significantly lower than the exact solution (39), consistent with a potential that is too attractive, on average. As such, the LGS wave function spreads out over multiple water molecules rather than forming an excluded volume.

That said, the LGS model does reproduce (at least qualitatively) a redshifting and broadening of the resonance Raman spectrum relative to that of neat liquid water (144), although it bears pointing out that the method used to compute the resonance Raman spectrum is based on a relationship between vibrational frequencies (computed using DFT) and electric fields along O–H bonds (computed using classical molecular dynamics) that was developed for neat liquid water (145). The appropriateness of this approach for negatively charged water is untested.

SUMMARY POINTS

1. Numerous computational and experimental studies have provided considerable insight regarding the underlying structure of small water cluster anions, but the complexity of the potential energy landscape makes definitive assignment of cluster spectra all but impossible except for the smallest clusters. Efforts are perhaps better directed at understanding spectroscopic trends in terms of the structure of the water network nearest the unpaired electron.

2. The vertical binding energy of $e^-(aq)$ has been characterized in bulk water using liquid microjet photoelectron spectroscopy, with results that are consistent with extrapolations of internally solvated $(H_2O)_N^-$ clusters, and with simulations of $e^-(aq)$ using both one- and many-electron theoretical methods.

3. Simulations strongly suggest that the hydrated electron at the air/water interface should be nearly indistinguishable, in terms of its optical spectrum and its vertical electron binding energy, from $e^-(aq)$ in bulk water, and indeed the aqueous electron may not even be stable at the air/water interface.

4. A cavity-forming, excluded-volume model of $e^-(aq)$ successfully rationalizes most (though not yet all) experimental data, often quantitatively or semiquantitatively. Within this model, the unpaired-electron hydrogen bonds to one O–H moiety from each of ≈ 4 water molecules, but with quantum-mechanical tails that extend ≈ 2 solvation shells.

DISCLOSURE STATEMENT

The authors are not aware of any affiliations, memberships, funding, or financial holdings that might be perceived as affecting the objectivity of this review.

ACKNOWLEDGMENTS

LITERATURE CITED

1. Thomas JM, Edwards PP, Kuznetsov VL. 2008. Sir Humphry Davy: boundless chemist, physicist, poet and man of action. *ChemPhysChem* 9:59–66

2. Weyl W. 1864. Ueber Metallammonium-Verbindungen. *Ann. Phys. Chem.* 197:601–12

3. Kraus CA. 1908. Solutions of metals in non-metallic solvents; II. On the formation of compounds between metals and ammonia. *J. Am. Chem. Soc.* 30:653–68

4. Kraus CA. 1907. Solutions of metals in non-metallic solvents; I. General properties of solutions of metals in liquid ammonia. *J. Am. Chem. Soc.* 29:1557–71

5. Kohlrausch F. 1876. Ueber das Leitungsvermogen der Wasergeloten Elektrolyte im Zusammenhang mit der Wanderung ihrer Bestandtheile. *Göttingen Nachrichten*, pp. 213–24. Engl. transl. HM Goodwin. 1899. *The Fundamental Laws of Electrolytic Conduction*. New York/London: Harper Brothers

6. Kraus CA. 1908. Solutions of metals in non-metallic solvents; IV. Material effects accompanying the passage of an electrical current through solutions of metals in liquid ammonia. Migration experiments. *J. Am. Chem. Soc.* 30:1323–44

7. Thompson JJ. 1897. Cathode rays. *Philos. Mag.* 44:293–316

8. Millikan RA. 1911. The isolation of an ion, a precision measurement of its charge, and the correction of Stokes's law. *Phys. Rev. (Ser. I)* 32:349–97

9. Gibson GE, Argo WL. 1916. The absorption spectra of the blue solutions of sodium and magnesium in liquid ammonia. *Phys. Rev.* 7:33–48

10. Gibson GE, Argo WL. 1918. The absorption spectra of the blue solutions of certain alkali and alkaline earth metals in liquid ammonia and in methylamine. *J. Am. Chem. Soc.* 40:1327–61

11. Ogg RA Jr. 1946. Physical interaction of electrons with liquid dielectric media. The properties of metal-ammonia solutions. *Phys. Rev.* 69:668–69

12. Jortner J. 1959. Energy levels of bound electrons in liquid ammonia. *J. Chem. Phys.* 30:839–46

13. Jortner J, Rice SA. 1965. Theoretical studies of solvated electrons. In *Solvated Electron*, *Adv. Chem.*, Vol. 50, ed. RF Gould, pp. 7–26. Washington, DC: Am. Chem. Soc.

14. Hart EJ, Anbar M. 1970. *The Hydrated Electron*. New York: Wiley-Intersci.

15. Boag JW. 1989. Pulse radiolysis: a historical account of the discovery of the optical absorption spectrum of the hydrated electron. In *Early Developments in Radiation Chemistry*, ed. J Kroh, pp. 7–20. Cambridge, UK: R. Soc. Chem.

16. Schuler RH. 1996. Radiation chemistry at Notre Dame 1943–1994. *Radiat. Phys. Chem.* 47:9–17

17. Stein G. 1952. Some aspects of the radiation chemistry of organic solutes. *Discuss. Faraday Soc.* 12:227–34

18. Walker DC. 1967. The hydrated electron. *Q. Rev. Chem. Soc.* 21:79–108

19. Hart EJ, Boag JW. 1962. Absorption spectrum of the hydrated electron in water and in aqueous solutions. *J. Am. Chem. Soc.* 84:4090–95

20. Dharmarathne L, Ashokkumar M, Grieser F. 2013. On the generation of the hydrated electron during sonolysis of aqueous solutions. *J. Phys. Chem. A* 117:2409–14

21. Martini IB, Barthel ER, Schwartz BJ. 2000. Mechanisms of the ultrafast production and recombination of solvated electrons in weakly polar fluids: comparison of multiphoton ionization and detachment via the charge-transfer-to-solvent transition of Na^- in THF. *J. Chem. Phys.* 113:11245–57

22. Kee TW, Son DH, Kambhampati P, Barbara PF. 2001. A unified electron transfer model for the different precursors and excited states of the hydrated electron. *J. Phys. Chem. A* 105:8434–39

23. Chen X, Bradforth SE. 2008. The ultrafast dynamics of photodetachment. *Annu. Rev. Phys. Chem.* 59:203–31

24. Buxton GV, Greenstock CL, Helman WP, Ross AB. 1988. Critical review of rate constants for reactions of hydrated electrons, hydrogen atoms and hydroxyl radicals ($^\bullet OH/^\bullet O$) in aqueous solution. *J. Phys. Chem. Ref. Data* 17:513–886

25. Garrett BC, Dixon DA, Camaioni DM, Chipman DM, Johnson MA, et al. 2005. Role of water in electron-initiated processes and radical chemistry: issues and scientific advances. *Chem. Rev.* 105:355–89

26. Copeland DA, Kestner NR, Jortner J. 1970. Excess electrons in polar solvents. *J. Chem. Phys.* 53:1189–216

27. Kestner NR, Jortner J. 1973. Radiative processes of the solvated electron in polar fluids. *J. Phys. Chem.* 77:1040–50

28. Fueki K, Feng DF, Kevan L, Christoffersen RE. 1971. A semicontinuum model for the hydrated electron. II. Configurational stability of the ground state. *J. Phys. Chem.* 75:2297–305

29. Feng DF, Kevan L. 1980. Theoretical models for solvated electrons. *Chem. Rev.* 80:1–20

30. Hentz RR, Farhataziz, Hansen EM. 1972. Pulse radiolysis of liquids at high pressures. III. Hydrated-electron reactions not controlled by diffusion. *J. Chem. Phys.* 57:2959–63

31. Borsarelli CD, Bertolotti SG, Previtali CM. 2003. Thermodynamic changes associated with the formation of the hydrated electron after photoionization of inorganic anions: a time-resolved photoacoustic study. *Photochem. Photobiol. Sci.* 2:791–95

32. Kevan L. 1981. Solvated electron structure in glassy matrices. *Acc. Chem. Res.* 14:138–45

33. Rossky PJ, Schnitker J. 1988. The hydrated electron: quantum simulation of structure, spectroscopy, and dynamics. *J. Phys. Chem.* 92:4277–85

34. Turi L, Rossky PJ. 2012. Theoretical studies of spectroscopy and dynamics of hydrated electrons. *Chem. Rev.* 112:5641–74

35. Boero M, Parrinello M, Terakura K, Ikeshoji T, Liew CC. 2003. First-principles molecular-dynamics simulations of a hydrated electron in normal and supercritical water. *Phys. Rev. Lett.* 90:226403

36. Boero M. 2007. Excess electron in water at different thermodynamic conditions. *J. Phys. Chem. A* 111:12248–56

37. Uhlig F, Marsalek O, Jungwirth P. 2012. Unraveling the complex nature of the hydrated electron. *J. Phys. Chem. Lett.* 3:3071–75

38. Larsen RE, Glover WJ, Schwartz BJ. 2010. Does the hydrated electron occupy a cavity? *Science* 329:65–69

39. Turi L, Madarász A. 2011. Comment on "Does the hydrated electron occupy a cavity?" *Science* 331:1387c

40. Jacobson LD, Herbert JM. 2011. Comment on "Does the hydrated electron occupy a cavity?" *Science* 331:1387d

41. Larsen RE, Glover WJ, Schwartz BJ. 2011. Response to comments on "Does the hydrated electron occupy a cavity?" *Science* 331:1387e

42. Herbert JM, Jacobson LD. 2011. Structure of the aqueous electron: assessment of one-electron pseudopotential models in comparison to experimental data and time-dependent density functional theory. *J. Phys. Chem. A* 115:14470–83

43. Armbruster M, Haberland H, Schindler HG. 1981. Negatively charged water clusters, or the first observation of free hydrated electrons. *Phys. Rev. Lett.* 47:323–26

44. Turi L, Sheu WS, Rossky PJ. 2005. Characterization of excess electrons in water-cluster anions by quantum simulations. *Science* 309:914–17

45. Verlet JRR, Bragg AE, Kammrath A, Cheshnovsky O, Neumark DM. 2005. Comment on "Characterization of excess electrons in water-cluster anions by quantum simulations." *Science* 310:1769b

46. Turi L, Sheu WS, Rossky PJ. 2005. Response to comment on "Characterization of excess electrons in water-cluster anions by quantum simulations." *Science* 310:1769c

47. Alizadeh E, Sanche L. 2012. Precursors of solvated electrons in radiobiological physics and chemistry. *Chem. Rev.* 112:5578–602

48. Marsalek O, Frigato T, VandeVondele J, Bradforth SE, Schmidt B, et al. 2010. Hydrogen forms in water by proton transfer to a distorted electron. *J. Phys. Chem. B* 114:915–20

49. Uhlig F, Jungwirth P. 2013. Embedded cluster models for reactivity of the hydrated electron. *Z. Phys. Chem.* 227:1583–93

50. Falcone JM, Becker D, Sevilla MD, Swarts SG. 2005. Products of the reactions of the dry and aqueous electron with hydrated DNA: hydrogen and 5,6-dihyropyrimidines. *Radiat. Phys. Chem.* 72:257–64

51. Alizadeh E, Sanz AG, García G, Sanche L. 2013. Radiation damage to DNA: the indirect effect of low-energy electrons. *J. Phys. Chem. Lett.* 4:820–25

52. Alizadeh E, Orlando TM, Sanche L. 2015. Biomolecular damage induced by ionizing radiation: the direct and indirect effects of low-energy electrons on DNA. *Annu. Rev. Phys. Chem.* 66:379–98

53. Boudaïffa B, Cloutier P, Hunting D, Huels MA, Sanche L. 2000. Resonance formation of DNA strand breaks by low-energy (3 to 20 eV) electrons. *Science* 287:1658–60

34. Review of simulations using pseudopotential models.

52. Review of electron damage to DNA.

54. Simons J. 2006. How do low-energy (0.1–2 eV) electrons cause DNA strand breaks? *Acc. Chem. Res.* 39:772–79

55. Wang CR, Nguyen J, Lu QB. 2009. Bond breaks of nucleotides by dissociative electron transfer of nonequilibrium prehydrated electrons: a new molecular mechanism for reductive DNA damage. *J. Am. Chem. Soc.* 131:11320–22

56. Gu J, Xie Y, Schaefer HF III. 2006. Electron attachment to nucleotides in aqueous solution. *ChemPhysChem* 7:1885–87

57. Smyth M, Kohanoff J. 2011. Excess electron localization in solvated DNA bases. *Phys. Rev. Lett.* 106:238108

58. Coe JV, Lee GH, Eaton JG, Arnold ST, Sarkas HW, et al. 1990. Photoelectron spectroscopy of hydrated electron cluster anions, $(H_2O)^-_{n=2-69}$. *J. Chem. Phys.* 92:3960–62

59. Verlet JRR, Bragg AE, Kammrath A, Cheshnovsky O, Neumark DM. 2005. Observation of large water-cluster anions with surface-bound excess electrons. *Science* 307:93–96

60. Ma L, Majer K, Chirot F, von Issendorff B. 2009. Low temperature photoelectron spectra of water cluster anions. *J. Chem. Phys.* 131:144303

61. Hammer NI, Roscioli JR, Bopp JC, Headrick JM, Johnson MA. 2005. Vibrational predissociation spectroscopy of the $(H_2O)^-_{6-21}$ clusters in the OH stretching region: evolution of the excess electron-binding signature into the intermediate cluster size regime. *J. Chem. Phys.* 123:244311

62. Asmis KR, Santabrogio G, Zhou J, Garand E, Headrick J, et al. 2007. Vibrational spectroscopy of hydrated electron clusters $(H_2O)^-_{15-50}$ via infrared multiple photon dissociation. *J. Chem. Phys.* 126:191105

63. Bailey CG, Kim J, Johnson MA. 1996. Infrared spectroscopy of the hydrated electron clusters $(H_2O)^-_n$, $n = 6$, 7: evidence for hydrogen bonding to the excess electron. *J. Phys. Chem.* 100:16782–85

64. Kim KS, Park I, Lee S, Cho K, Lee JY, et al. 1996. The nature of a wet electron. *Phys. Rev. Lett.* 76:956–59

65. Lee S, Kim J, Lee SJ, Kim KS. 1997. Novel structures for the excess electron state of the water hexamer and the interaction forces governing the structure. *Phys. Rev. Lett.* 79:2038–41

66. Ayotte P, Weddle GH, Bailey CG, Johnson MA, Vila F, Jordan KD. 1999. Infrared spectroscopy of negatively charged water clusters: evidence for a linear network. *J. Chem. Phys.* 110:6268–77

67. Lee HM, Lee S, Kim KS. 2003. Structures, energetics, and spectra of electron–water clusters, e^-–$(H_2O)_{2-6}$ and e^-–$HOD(D_2O)_{1-5}$. *J. Chem. Phys.* 119:187–94

68. Lee S, Lee SJ, Lee JY, Kim J, Kim KS, et al. 1996. Ab initio study of water hexamer anions. *Chem. Phys. Lett.* 254:128–34

69. Weigend F, Ahlrichs R. 1999. Ab initio treatment of $(H_2O)^-_2$ and $(H_2O)^-_6$. *Phys. Chem. Chem. Phys.* 1:4537–50

70. Hammer NI, Roscioli JR, Johnson MA. 2005. Identification of two distinct electron binding motifs in the anionic water clusters: a vibrational spectroscopic study of the $(H_2O)^-_6$ isomers. *J. Phys. Chem. A* 109:7896–901

71. Hammer NI, Shin JW, Headrick JM, Diken EG, Roscioli JR, et al. 2004. How do small water clusters bind an excess electron? *Science* 306:675–79

72. Herbert JM. 2015. The quantum chemistry of loosely bound electrons. In *Reviews in Computational Chemistry*, Vol. 28, eds. AL Parill, K Lipkowitz, pp. 391–517. Hoboken, NJ: John Wiley & Sons

73. Sommerfeld T, Gardner SD, DeFusco A, Jordan KD. 2006. Low-lying isomers and finite temperature behavior of $(H_2O)^-_6$. *J. Chem. Phys.* 125:174301

74. Choi TH, Jordan KD. 2009. Potential energy landscape of the $(H_2O)^-_6$ cluster. *Chem. Phys. Lett.* 475:293–97

75. Roscioli JR, Hammer NI, Johnson MA, Diri K, Jordan KD. 2008. Exploring the correlation between network structure and electron binding energy in the $(H_2O)^-_7$ cluster through isomer-photoselected vibrational predissociation spectroscopy and ab initio calculations: addressing complexity beyond types I–III. *J. Chem. Phys.* 128:104314

76. Guasco TL, Elliott BM, Johnson MA, Ding J, Jordan KD. 2010. Isolating the spectral signatures of individual sites in water networks using vibrational double-resonance spectroscopy of cluster isotopomers. *J. Phys. Chem. Lett.* 1:2396–401

59. Experimental demonstration of the existence of multiple isomers in water cluster anions.

71. Experimental observation of the AA isomer in water cluster anions.

72. Extensive review of anion quantum chemistry.

Amu. Rev. Phys. Chem. 2017.68:447-472. Downloaded from www.annualreviews.org
Access provided by Ohio State University Library on 05/03/17. For personal use only.

77. Herbert JM, Head-Gordon M. 2006. Charge penetration and the origin of large O–H vibrational red-shifts in hydrated-electron clusters, $(H_2O)_n^-$. *J. Am. Chem. Soc.* 128:13932–39

78. Diken EG, Robertson WH, Johnson MA. 2004. The vibrational spectrum of the neutral $(H_2O)_6$ precursor to the "magic" $(H_2O)_6^-$ cluster anion by argon-mediated, population-modulated electron attachment spectroscopy. *J. Phys. Chem. A* 108:64–68

79. Barnett RN, Landman U, Cleveland CL, Jortner J. 1988. Electron localization in water clusters. II. Surface and internal states. *J. Chem. Phys.* 88:4429–47

80. Barnett RN, Landman U, Scharf D, Jortner J. 1989. Surface and internal excess electron states in molecular clusters. *Acc. Chem. Res.* 22:350–57

81. Herbert JM, Head-Gordon M. 2005. Calculation of electron detachment energies for water cluster anions: An appraisal of electronic structure methods, with application to $(H_2O)_{20}^-$ and $(H_2O)_{24}^-$. *J. Phys. Chem. A* 109:5217–29

82. Williams CF, Herbert JM. 2008. Influence of structure on electron correlation effects and electron–water dispersion interactions in anionic water clusters. *J. Phys. Chem. A* 112:6171–78

83. Jacobson LD, Herbert JM. 2010. A one-electron model for the aqueous electron that includes many-body electron-water polarization: bulk equilibrium structure, vertical electron binding energy, and optical absorption spectrum. *J. Chem. Phys.* 133:154106

84. Kim J, Becker I, Cheshnovsky O, Johnson MA. 1998. Photoelectron spectroscopy of the "missing" hydrated electron clusters $(H_2O)_n^-$, n = 3, 5, 8, and 9: isomers and continuity with the dominant clusters n = 6, 7 and 11. *Chem. Phys. Lett.* 297:90–96

85. Shin JW, Hammer NI, Headrick JM, Johnson MA. 2004. Preparation and photoelectron spectrum of the 'missing' $(H_2O)_4^-$ cluster. *Chem. Phys. Lett.* 399:349–53

86. Makov G, Nitzan A. 1994. Solvation and ionization near a dielectric surface. *J. Phys. Chem.* 98:3459–66

87. Kammrath A, Verlet JRR, Griffin GB, Neumark DM. 2006. Photoelectron spectroscopy of large (water)$_n^-$ (n = 50–200) clusters at 4.7 eV. *J. Chem. Phys.* 125:076101

88. Jacobson LD, Williams CF, Herbert JM. 2009. The static-exchange electron-water pseudopotential, in conjunction with a polarizable water model: a new Hamiltonian for hydrated-electron simulations. *J. Chem. Phys.* 130:124115

89. **Jacobson LD, Herbert JM. 2011. Theoretical characterization of four distinct isomer types in hydrated-electron clusters, and proposed assignments for photoelectron spectra of water cluster anions. *J. Am. Chem. Soc.* 133:19889–99**

90. **Marsalek O, Uhlig F, VandeVondele J, Jungwirth P. 2012. Structure, dynamics, and reactivity of hydrated electrons by ab initio molecular dynamics. *Acc. Chem. Res.* 45:23–32**

91. Uhlig F, Herbert JM, Coons MP, Jungwirth P. 2014. Optical spectroscopy of the bulk and interfacial hydrated electron from ab initio calculations. *J. Phys. Chem. A* 118:7507–15

92. **Kumar A, Walker JA, Bartels DM, Sevilla MD. 2015. A simple ab initio model for the hydrated electron that matches experiment. *J. Phys. Chem. A* 119:9148–59**

93. Tauber MJ, Mathies RA. 2003. Structure of the aqueous solvated electron from resonance Raman spectroscopy: lessons from isotopic mixtures. *J. Am. Chem. Soc.* 125:1394–402

94. Turi L, Borgis D. 2002. Analytical investigations of an electron–water molecule pseudopotential. II. Development of a new pair potential and molecular dynamics simulations. *J. Chem. Phys.* 117:6186–95

95. **Jacobson LD, Herbert JM. 2010. Polarization-bound quasi-continuum states are responsible for the 'blue tail' in the optical absorption spectrum of the aqueous electron. *J. Am. Chem. Soc.* 132:10000–2**

96. Tang Y, Shen H, Sekiguchi K, Kurahashi N, Mizuno T, et al. 2010. Direct measurement of vertical binding energy of a hydrated electron. *Phys. Chem. Chem. Phys.* 12:3653–55

97. Shreve AT, Yen TA, Neumark DM. 2010. Photoelectron spectroscopy of hydrated electrons. *Chem. Phys. Lett.* 493:216–19

98. Lübcke A, Buchner F, Heine N, Hertel IV, Schultz T. 2010. Time-resolved photoelectron spectroscopy of solvated electrons in aqueous NaI solution. *Phys. Chem. Chem. Phys.* 12:14629–34

99. Siefermann KR, Liu Y, Lugovoy E, Link O, Faubel M, et al. 2010. Binding energies, lifetimes and implications of bulk and interface solvated electrons in water. *Nat. Phys.* 2:274–79

100. Buchner F, Schultz T, Lübcke A. 2012. Solvated electrons at the water-air interface: surface versus bulk signal in low kinetic energy photoelectron spectroscopy. *Phys. Chem. Chem. Phys.* 14:5837–42

101. Yamamoto Y, Karashima S, Adachi S, Suzuki T. 2016. Wavelength dependence of UV photoemission from solvated electrons in bulk water, methanol, and ethanol. *J. Phys. Chem. A* 120:1153–59

102. Coe JV, Williams SM, Bowen KH. 2008. Photoelectron spectra of hydrated electron clusters versus cluster size. *Int. Rev. Phys. Chem.* 27:27–51

103. Stähler J, Deinert JC, Wegkamp D, Hagen S, Wolf M. 2015. Real-time measurement of the vertical binding energy during the birth of a solvated electron. *J. Am. Chem. Soc.* 137:3520–24

104. Signorell R, Goldmann M, Yoder BL, Andras B, Chasovskikh E, et al. 2016. Nanofocusing, shadowing, and electron mean free path in the photoemission from aerosol droplets. *Chem. Phys. Lett.* 658:1–6

105. Elkins MH, Williams HL, Shreve AT, Neumark DM. 2013. Relaxation mechanism of the hydrated electron. *Science* 342:1496–99

106. Karashima S, Yamamoto, Y, Suzuki T. 2016. Resolving nonadiabatic dynamics of hydrated electrons using ultrafast photoemission anisotropy. *Phys. Rev. Lett.* 116:137601

107. Siefermann KR, Abel B. 2011. The hydrated electron: a seemingly familiar chemical and biological transient. *Angew. Chem. Int. Ed. Engl.* 50:5264–72

108. Abel B, Buck U, Sobolewski AL, Domcke W. 2012. On the nature and signatures of the solvated electron in water. *Phys. Chem. Chem. Phys.* 14:22–34

109. Faubel M, Siefermann KR, Liu Y, Abel B. 2012. Ultrafast soft X-ray photoelectron spectroscopy at liquid water microjets. *Acc. Chem. Res.* 45:120–30

110. Abel B. 2013. Hydrated interfacial ions and electrons. *Annu. Rev. Phys. Chem.* 64:533–52

111. Coons MP, You ZQ, Herbert JM. 2016. The hydrated electron at the interface of neat liquid water appears to be indistinguishable from the bulk species. *J. Am. Chem. Soc.* 138:10879–86

112. Casey JR, Schwartz BJ, Glover WJ. 2016. Free energies of cavity and noncavity hydrated electrons near the instantaneous air/water interface. *J. Phys. Chem. Lett.* 7:3192–98

113. Bovensiepen U, Gahl C, Stähler J, Bockstedte M, Meyer M, et al. 2009. A dynamic landscape from femtoseconds to minutes for excess electrons at ice–metal interfaces. *J. Phys. Chem. C* 113:979–88

114. Bertin M, Meyer M, Stähler J, Gahl C, Wolf M, Bovensiepen U. 2009. Reactivity of water–electron complexes on crystalline ice surfaces. *Faraday Discuss.* 141:293–307

115. Lu QB, Sanche L. 2001. Effects of cosmic rays on atmospheric chloroflurocarbon dissociation and ozone depletion. *Phys. Rev. Lett.* 87:078501

116. Lu QB. 2010. Cosmic-ray-driven electron-induced reactions of halogenated molecules adsorbed on ice surfaces: implications for atmospheric ozone depletion and global climate change. *Phys. Rep.* 487:141–67

117. Müller R. 2003. Impact of cosmic rays on stratospheric chlorine chemistry and ozone depletion. *Phys. Rev. Lett.* 91:058502

118. Müller R, Grooß JU. 2009. Does cosmic-ray-induced heterogeneous chemistry influence stratospheric polar ozone loss? *Phys. Rev. Lett.* 103:228501

119. Grooß JU, Müller R. 2011. Do cosmic-ray-driven electron-induced reactions impact stratospheric ozone depletion and global climate change? *Atmos. Environ.* 45:3508–14

120. Golden S, Guttman C, Tuttle TR Jr. 1966. Species and composition of dilute alkali-metal–ammonia solutions. *J. Chem. Phys.* 44:3791–96

121. Golden S, Tuttle TR Jr. 1978. On the nature of solvated electrons in polar fluids. *J. Phys. Chem.* 82:944–51

122. Sagar DM, Bain CD, Verlet JRR. 2010. Hydrated electrons at the water/air interface. *J. Am. Chem. Soc.* 132:6917–19

123. Matsuzaki K, Kusaka R, Nihonyanagi S, Yamaguchi S, Nagata T, Tahara T. 2016. Partially hydrated electrons at the air/water interface observed by UV-excited time-resolved heterodyne-detected vibrational frequency generation spectroscopy. *J. Am. Chem. Soc.* 138:7551–57

124. Bartels DM, Takahashi K, Cline JA, Marin TW, Jonah CD. 2005. Pulse radiolysis of supercritical water. 3. Spectrum and thermodynamics of the hydrated electron. *J. Phys. Chem. A* 109:1299–307

125. Coe JV, Arnold ST, Eaton JG, Lee GH, Bowen KH. 2006. Photoelectron spectra of hydrated electron clusters: fitting line shapes and grouping isomers. *J. Chem. Phys.* 125:014315

102. Thorough analysis of cluster photoelectron spectra.

126. Turi L, Hantal G, Rossky PJ, Borgis D. 2009. Nuclear quantum effects in electronically adiabatic quantum time correlation functions: application to the absorption spectrum of a hydrated electron. *J. Chem. Phys.* 131:024119

127. Golden S, Tuttle TR Jr. 1979. Nature of solvated electron absorption spectra. *J. Chem. Soc. Faraday Trans. 2* 75:474–84

128. Coe JV. 2001. Fundamental properties of bulk water from cluster ion data. *Int. Rev. Phys. Chem.* 20:33–58

129. Golden S, Tuttle TR Jr. 1981. Shape stability of solvated-electron optical absorption bands. Part 2.—Theoretical implication. *J. Chem. Soc. Faraday Trans. 2* 77:889–97

130. Herbert JM, Jacobson LD. 2011. Nature's most squishy ion: the important role of solvent polarization in the description of the hydrated electron. *Int. Rev. Phys. Chem.* 30:1–48

131. Hare PM, Price EA, Stanisky CM, Janik I, Bartels DM. 2010. Solvated electron extinction coefficient and oscillator strength in high temperature water. *J. Phys. Chem. A* 114:1766–75

132. Schlick S, Narayana PA, Kevan L. 1976. ESR line shape studies of trapped electrons in γ-irradiated ^{17}O enriched 10 M NaOH alkaline ice glass: model for the geometrical structure of the trapped electron. *J. Chem. Phys.* 64:3153–60

133. Savolainen J, Uhlig F, Ahmed S, Hamm P, Jungwirth P. 2014. Direct observation of the collapse of the delocalized excess electron in water. *Nat. Phys.* 6:697–701

134. Tay KA, Boutin A. 2009. Hydrated electron diffusion: the importance of hydrogen-bond dynamics. *J. Phys. Chem. B* 113:11943–49

135. Tuckerman ME, Marx D, Parrinello M. 2002. The nature and transport mechanism of hydrated hydroxide ions in aqueous solution. *Nature* 417:925–29

136. Hameka HF, Robinson GW, Marsden CJ. 1987. Structure of the hydrated electron. *J. Phys. Chem.* 91:3150–57

137. Khatib R, Hasegawa T, Sulpizi M, Backus EHG, Bonn M, et al. 2016. Molecular dynamics simulations of SFG librational modes spectra of water at the water–air interface. *J. Phys. Chem. C* 120:18665–73

138. Shkrob IA. 2007. The structure of the hydrated electron. Part 1. Magnetic resonance of internally trapping water anions: a density functional theory study. *J. Phys. Chem. A* 111:5223–31

139. Tuttle TR Jr., Golden S. 1991. Solvated electrons: What is solvated? *J. Phys. Chem.* 95:5725–36

140. Clementi E, McLean AD, Ratmondi DL, Yoshimine M. 1964. Atomic negative ions. Second period. *Phys. Rev.* 133:A1274–79

141. Sobolewski AL, Domcke W. 2002. Hydrated hydronium: a cluster model of the solvated electron? *Phys. Chem. Chem. Phys.* 4:4–10

142. Neumann S, Eisfeld W, Sobolewski A, Domcke W. 2004. Simulation of the resonance Raman spectrum of the hydrated electron in the hydrated-hydronium cluster model. *Phys. Chem. Chem. Phys.* 6:5297–303

143. Hentz RR, Farhataziz, Hansen EM. 1972. Pulse radiolysis of liquids at high pressures. II. Diffusion-controlled reactions of the hydrated electron. *J. Chem. Phys.* 56:4485–88

144. Casey JR, Larsen RE, Schwartz BJ. 2013. Resonance Raman and temperature-dependent electronic absorption spectra of cavity and noncavity models of the hydrated electron. *PNAS* 110:2712–17

145. Corcelli SA, Skinner JL. 2005. Infrared and Raman line shapes of dilute HOD in liquid H_2O and D_2O from 10 to 90°C. *J. Phys. Chem. A* 109:6154–65